Supplementary Information

Nanoscopic Terraces, Mesas and Ridges in Freely-Standing Thin Films Sculpted by Supramolecular Oscillatory Surface Forces

Yiran Zhang, Subinuer Yilixiati, Collin Pearsall and Vivek Sharma*

Department of Chemical Engineering, University of Illinois at Chicago, Chicago, IL 60607.

In the present note, additional information is provided regarding the imaging technique and image analysis. Both DLVO and non-DLVO supramolecular contributions to disjoining pressure in the foams films made with aqueous SDS solutions are described and the representative thickness dependent disjoining pressure is plotted for two micellar solutions.

S1. Imaging system

The IDIOM method can be realized with a variety of cameras and light sources. To illustrate this, we carried out the thickness measurement of stratifying foam films with three different cameras, including a commercial, consumer-grade digital camera. The properties of the cameras are listed in Table S1. Two light sources are also used: a Fiilex P360EX LED light and a Schott ACE 1 halogen light. The thicknesses of stratification layers are recovered (similar to Figure. 1(a) in the main text), using all cameras and light sources.

High-resolution videos and images of the stratification process are captured by this imaging system. The images are post-processed in MATLAB R2014a with specially written codes and using Equation 1 (see main article), changes in the film thickness are computed from the intensity of reflected light. While similar digital filtration and thickness determination via reflected light intensity has been used for measuring film thicknesses with thicker, colored soap

films, [1, 2] we extend the application to thicknesses below 100 nm, and to determination of topographical map of thickness. The thickness computed using Equation 1 is an "equivalent film thickness" obtained by assuming that the refractive index of thin film is same as that of the bulk fluid. Prior studies[3-5] show that corrections based on the measured refractive index for different SDS concentrations, or based on calculations that treat foam as a multilayered structure are negligible and can be ignored. Through an extensive literature survey, we were able to find several examples of the use of consumer-grade, off-the-shelf DSLR cameras a photometers, spectrophotometers, colorimeters and photodiodes in star gazing and astronomy,[6-8] contrasting color of polymer nanocomposites made with gold nanoparticles dispersed in a polymer matrix,[9, 10] detection of fluorophores in so-called photoscopy applications,[11] forensic investigations,[12] and for investigation of colors in biology.[13-16] In the present study, we are able to quantitatively analyze the nanoscopic topographic structures in freely-standing foam films with a variety of cameras.

Table S1. List of cameras tested with IDIOM protocol

Camera name	Record format	Bit depth	Pixel resolution	Frame rate (fps)
Photron FASTCAM Mini UX100	High speed movie (.mraw)	12	1280*1024	Up to 4000 (full frame)
Tucsen ISH1000 CCD	Movie (.avi)	8	3664*2748	~3 (full frame)
Nikon D5200 DSLR	RAW image (.nef)*	14	6000*4000	~1
	Movie (.mov)**	8	1920*1080	30

* The RAW images are converted to .tiff without compression using open source program DCRaw. The resulting .tiff images are analyzed with specially written code in MATLAB.
** The movie format in the consumer camera applies a lossy compression, resulting in a non-linear relation between output RGB values and the actual light intensity. This non-linear compression is taken into account through careful intensity vs. RGB output calibration.

Finally we discuss the theoretical limits of the IDIOM method. In an ideal case, the camera converts light intensity with no signal noise, and utilizes its entire dynamic range (*i.e.*, $I_{\max} = 2^{BitDepth} - 1$, $I_{\min} = 0$ in calculating Δ in Equation 1 in the main text). The intrinsic minimum measurable thickness and measurement error are then results of the quantization of light intensity to integer values as RGB output. With different camera bit depth, the available number of integers varies as $2^{BitDepth}$. Therefore the theoretical thickness resolution and lower limit of the measurement vary. For each color channel, the minimum measurable thickness is reached when the light intensity is enough to be distinguished from the background, *i.e.* $I - I_{\min} = 1$. The intrinsic error ε associated with rounding up the light intensity to integer RGB values can be estimated by

$$\varepsilon(I) = \frac{h(I+0.5) - h(I-0.5)}{2} \tag{S1}$$

Where $h(I \pm 0.5)$ is computed by using Equation 1 in the main text. Due to the inherent non-linear nature of the Equation 1, the error is different at different thickness. As shown in Figure S1, it approaches maximum when the intensity is close to the extrema. The minimum measurable thickness (reached in blue channel) and the maximum error (reached in red channel) are listed in Table S2 for several bit depths for typical cameras.

As shown in Table S2, even with low camera bit depth, IDIOM method could measure thicknesses well below 10 nm with reasonable accuracy. However, the discussion above is based on an ideal case, and aimed to find the limits of the IDIOM method in the best case. In real experiments, outside stray light, imperfect lenses and noises of CCD or CMOS camera sensors can all contribute to errors in determining intensity *I*. On the other hand, intensity acquired in

single pixel can be averaged both spatially and temporally to reduce the noise. Error can also come in determining interference extrema I_{max} and I_{min}, which are measured with care and averaged from multiple measurements. Possible error could originate from the digital filtration, since we use a single averaged wavelength value for each color channel, while the actual filtered light has a spectrum of wavelengths near the averaged value. However, we recognize that the thickness is linearly proportional to the wavelength ($h \propto \lambda$, see Equation 1 main text), so an uncertainty in wavelength of ±10 nm would only result in a ~2% relative uncertainty (λ~500 nm) in estimated thickness.

Table S2. Ideal minimum measurable thickness and maximum intrinsic error in IDIOM method

Bit depth	Intensity levels	Minimum measurable thickness [nm]	Maximum intrinsic error [nm]
8	0 - 255	3.39	1.31
12	0 - 4095	0.84	0.33
14	0 - 16383	0.42	0.16
16	0 - 65535	0.21	0.08

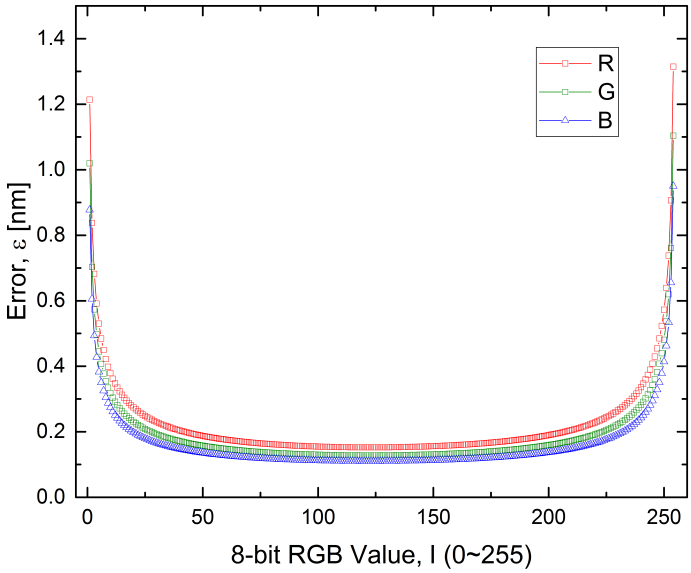

Figure S1. The intrinsic error, ε vs. RGB intensity, I, computed by Eqn. S1 for a 8-bit camera. The intrinsic error in thickness measurement is associated with rounding up light intensity to integer values as RGB output.

S2. Supramolecular Oscillatory Structural Contribution to Disjoining Pressure

The simplest expression for disjoining Pressure $\Pi(h)$ includes the two contributions by dispersion forces (van der Waals attraction) $\Pi_{vw}(h)$ and electrostatic double layer repulsion, $\Pi_{el}(h)$ that are invoked together in the DLVO theory of colloidal stability. Additional non-DLVO supramolecular oscillatory structural forces $\Pi_{os}(h)$ can arise in thin films made with particles, micelles and polyelectrolytes due to confinement-induced layering of these structures. Here we describe the typical values of disjoining pressure, to highlight how the supramolecular structural force contribution underlies the formation of stratified foam films. Several reviews, papers and texts can be consulted for detailed arguments and discussion.[17-27] We primarily use the equations and assumptions from a paper by Anachkov, Danov, Basheva, Kralchevsky and Ananthapadmanabhan.[22]

The disjoining pressure within a foam film can be described as a sum of different contributions including van der Waal dispersion forces, electrostatic double layer forces and supramolecular oscillatory forces. The relevant parameters, corresponding symbols and their characteristic values are listed in the Table S3 and Table S4, and the contributions are plotted in Figure S2.

$$\Pi(h) = \Pi_{vw}(h) + \Pi_{el}(h) + \Pi_{os}(h) \tag{S2}$$

The van der Waals contribution[22, 24] can be calculated by using a thickness dependent Hamaker constant $A(h)$, and the following expressions:

$$\Pi_{vw}(h) = -\frac{A(h)}{6\pi h^3} \tag{S3a}$$

$$A = 2\kappa h A_0 \exp(-2\kappa h) + \frac{3h_p v_e}{4\pi} \frac{(n_w^2-1)^2}{(n_w^2+1)^{3/2}} \int_0^\infty \frac{(1+2\hat{h}z)}{(1+2z^2)^2} \exp(-2\hat{h}z) dz \tag{S3b}$$

$$\hat{h} = 2\pi v_e h n_w (n_w^2+1)^{1/2} / c_0 \tag{S3c}$$

In the electrolyte solution, ‘’zero-frequency” contribution A_0 to the Hamaker constant is negligible. Therefore the van der Waals attraction is only dependent on dispersion forces.[24] The electrostatic component of disjoining pressure can be calculated through osmotic pressure difference in the film[28, 29] by using the following expressions.

$$\Pi_{el} = (P_{osm})_{midplane} - (P_{osm})_{bulk} \tag{S4a}$$

$$(P_{osm})_{bulk} = kT[2(c_1+c_3)+(Z+1)c_p] \tag{S4b}$$

$$(P_{osm})_{midplane} = kT[(c_1+c_3)(e^{\Phi_m}+e^{-\Phi_m})+Zc_p e^{\Phi_m}+c_p e^{-Z\Phi_m}] \tag{S4c}$$

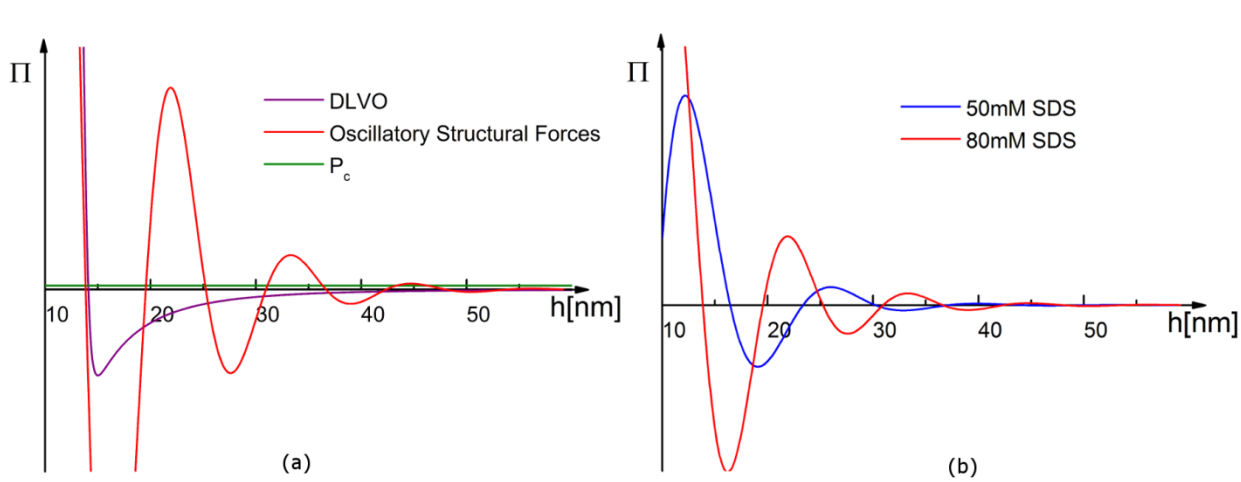

Figure S2 **Intermolecular and surface forces in the thin film**. **(a)** Contributions to the disjoining pressure in 80Mm SDS thin film are shown. The DLVO forces calculated using $\Pi_{DLVO}(h) = \Pi_{vw}(h) + \Pi_{el}(h)$ are decay at a thickness of 30 nm while the supramolecular oscillatory structural forces are longer ranged. **(b)** Concentration-dependence of supramolecular oscillatory structural forces is shown using calculated value for 50 mM and 80 mM.

The Zc_p term describes concentration of dissociated ions. Φ_m is the dimensionless electrostatic mid-plane potential, $\Phi_m = \frac{e|\psi_m|}{kT}$ that is obtained by solving Poisson-Boltzmann equation given below numerically.

$$\frac{d^2\Phi}{dx^2} = 4\pi L_B[2(c_1 + c_3)\sinh\Phi + Zc_p(e^{\Phi} - e^{-Z\Phi})] \tag{S5}$$

Finally the supramolecular oscillatory structural force contributions are computed using the following expressions [30].

$$\Pi_{os} = P_0 \cos(\frac{2\pi h}{d_1})\exp(\frac{d^3}{d_1^2 d_2} - \frac{h}{d_2}) \text{ , for } h > d \tag{S6a}$$

$$\Pi_{os} = -P_0 \text{ , for } 0 < h < d \tag{S6b}$$

$$P_0 = \rho kT \frac{1 + \varphi + \varphi^2 - \varphi^3}{(1-\varphi)^3} \qquad \rho = \frac{6\varphi}{\pi d^3} \tag{S6c}$$

Table S3 Parameters, symbols and values used in calculation of representative disjoining pressure.

Parameter	Symbol	Value
Film thickness	h	10-60 nm
Hamaker constant	A	10^{-19} J
Planck constant	h_p	6.63×10^{-34} J·s
Main electronic absorption frequency	v_e	3×10^{15} Hz
Speed of light in vacuum	c_0	3.0×10^{8} m/s
Refractive index of water	n_w	1.333
Boltzmann constant	k	1.3806×10^{-23} m^2 kg s^{-2} K^{-1}
Temperature	T	298.15 K
Number density of surfactant monomers	c_1	CMC×N_A
Number density of added electrolyte	c_3	0
Number density of micelles	c_p	$(c-CMC)\times N_A / N_{agg}$
Charge of the macroions	Z	35-37
Bjerrum length	L_B	0.72 nm
Thickness of two adsorption layers at the film	h_a	5.26 nm
Aggregation number	N_{agg}	65
Dimensionless surface potential	Φ_s	5.5

Table S4 Concentration dependent parameters used in calculation of representative disjoining pressure.*

Concentration (mM)	Period d_1 (nm)	Debye length κ^{-1} (nm)	Volume fraction φ	Effective micelle diameter d (nm)	Decay length d_2 (nm)
50	13.84	2.67	0.190	12.12	5.62
60	12.89	2.52	0.219	11.23	5.75
80	11.56	2.31	0.267	10.64	6.45
100	10.65	2.16	0.307	9.92	6.96

*In the table, d_1, κ^{-1} are calculated based on ref [28]; d_2, d, φ are calculated based on ref [30].

REFERENCES

1. Karakashev, S. I.; Nguyen, A. V.; Manev, E. D. A Novel Technique for Improving Interferometric Determination of Emulsion Film Thickness by Digital Filtration. *J. Colloid Interface Sci.* 2007, 306, 449-453.
2. Sett, S.; Sinha-Ray, S.; Yarin, A. L. Gravitational Drainage of Foam Films. *Langmuir* 2013, 29, 4934-4947.
3. Adelizzi, E. A.; Troian, S. M. Interfacial Slip in Entrained Soap Films Containing Associating Hydrosoluble Polymer. *Langmuir* 2004, 20, 7482-7492.
4. Berg, S.; Adelizzi, E. A.; Troian, S. M. Experimental Study of Entrainment and Drainage Flows in Microscale Soap Films. *Langmuir* 2005, 21, 3867-3876.
5. Sheludko, A. Thin Liquid Films. *Adv. Colloid Interface Sci.* 1967, 1, 391-464.
6. Hoot, J. E. In *Photometry with Dslr Cameras*, Society for Astronomical Sciences Annual Symposium, 2007; p 67.
7. Jensen, T. J. *Budget Astrophotography: Imaging with Your Dslr or Webcam*. Springer: 2014.
8. Kloppenborg, B. K.; Pieri, R.; Eggenstein, H.-B.; Maravelias, G.; Pearson, T. A Demonstration of Accurate Wide-Field V-Band Photometry Using a Consumer-Grade Dslr Camera 2013, p. arXiv:1303.6870.
9. Sharma, V. Colloidal Gold Nanorods, Iridescent Beetles and Breath Figure Templated Assembly of Ordered Array of Pores in Polymer Films. Ph. D. Thesis, Georgia Institute of Technology, Atlanta, GA, 2008.
10. Sharma, V.; Park, K.; Srinivasarao, M. Colloidal Dispersion of Gold Nanorods: Historical Background, Optical Properties, Seed-Mediated Synthesis, Shape Separation and Self-Assembly. *Mater. Sci. Eng., R* 2009, 65, 1-38.
11. Schwaebel, T.; Menning, S.; Bunz, U. H. F. Photoscopy: Spectroscopic Information from Camera Snapshots? *Chem. Sci.* 2014, 5, 1422-1428.
12. Garcia, J. E.; Wilksch, P. A.; Spring, G.; Philp, P.; Dyer, A. Characterization of Digital Cameras for Reflected Ultraviolet Photography; Implications for Qualitative and Quantitative Image Analysis During Forensic Examination. *J. Forensic Sci.* 2014, 59, 117-122.
13. Sharma, V.; Crne, M.; Park, J. O.; Srinivasarao, M. Structural Origin of Circularly Polarized Iridescence in Jeweled Beetles. *Science* 2009, 325, 449-451.
14. Sharma, V.; Crne, M.; Park, J. O.; Srinivasarao, M. Bouligand Structures Underlie Circularly Polarized Iridescence of Scarab Beetles: A Closer View. *Mater. Today: Proceedings* 2014, 1, 161-171.
15. Pike, T. W. Using Digital Cameras to Investigate Animal Colouration: Estimating Sensor Sensitivity Functions. *Behav. Ecol. Sociobiol.* 2011, 65, 849-858.
16. Garcia, J. E.; Rohr, D.; Dyer, A. G. Trade-Off between Camouflage and Sexual Dimorphism Revealed by Uv Digital Imaging: The Case of Australian Mallee Dragons (Ctenophorus Fordi). *Journal of Experimental Biology* 2013, 216, 4290-4298.
17. Nikolov, A. D.; Wasan, D. T. Ordered Micelle Structuring in Thin Films Formed from Anionic Surfactant Solutions: I. Experimental. *J. Colloid Interface Sci.* 1989, 133, 1-12.
18. Nikolov, A. D.; Wasan, D. T. Wetting-Dewetting Films: The Role of Structural Forces. *Adv. Colloid Interface Sci.* 2014, 206, 207-221.
19. Bergeron, V. Forces and Structure in Thin Liquid Soap Films. *J. Phys.: Condens. Matter* 1999, 11, R215-R258.

20. Bergeron, V.; Jimenez-Laguna, A. I.; Radke, C. J. Hole Formation and Sheeting in the Drainage of Thin Liquid Films. *Langmuir* 1992, 8, 3027-3032.
21. Bergeron, V.; Langevin, D.; Asnacios, A. Thin-Film Forces in Foam Films Containing Anionic Polyelectrolyte and Charged Surfactants. *Langmuir* 1996, 12, 1550-1556.
22. Anachkov, S. E.; Danov, K. D.; Basheva, E. S.; Kralchevsky, P. A.; Ananthapadmanabhan, K. P. Determination of the Aggregation Number and Charge of Ionic Surfactant Micelles from the Stepwise Thinning of Foam Films. *Adv. Colloid Interface Sci.* 2012.
23. Basheva, E. S.; Kralchevsky, P. A.; Danov, K. D.; Ananthapadmanabhan, K. P.; Lips, A. The Colloid Structural Forces as a Tool for Particle Characterization and Control of Dispersion Stability. *Phys. Chem. Chem. Phys.* 2007, 9, 5183-5198.
24. Israelachvili, J. N. *Intermolecular and Surface Forces*. 3rd ed.; Academic Press: 2011.
25. von Klitzing, R.; Thormann, E.; Nylander, T.; Langevin, D.; Stubenrauch, C. Confinement of Linear Polymers, Surfactants, and Particles between Interfaces. *Adv. Colloid Interface Sci.* 2010, 155, 19-31.
26. Stubenrauch, C.; von Klitzing, R. Disjoining Pressure in Thin Liquid Foam and Emulsion Films—New Concepts and Perspectives. *J. Phys.: Condens. Matter* 2003, 15, R1197.
27. Cantat, I.; Cohen-Addad, S.; Elias, F.; Graner, F.; Höhler, R.; Pitois, O. *Foams: Structure and Dynamics*. Oxford University Press: 2013.
28. Danov, K. D.; Basheva, E. S.; Kralchevsky, P. A.; Ananthapadmanabhan, K. P.; Lips, A. The Metastable States of Foam Films Containing Electrically Charged Micelles or Particles: Experiment and Quantitative Interpretation. *Adv. Colloid Interface Sci.* 2011, 168, 50-70.
29. Fennell Evans, D.; Wennerström, H. *The Colloidal Domain: Where Physics, Chemistry, Biology, and Technology Meet*. 2nd ed.; Wiley-VCH: New York: 1999.
30. Kralchevsky, P. A.; Denkov, N. D. Analytical Expression for the Oscillatory Structural Surface Force. *Chem. Phys. Lett.* 1995, 240, 385-392.